DOI:10.1021/ic900345s

Inorganic Chemistry
Article

1D Coordination Polymers Constructed from anti−anti Carboxylato-Bridged $Mn_3^{III}O(Brppz)_3$ Units: From Long-Range Magnetic Ordering to Single-Chain Magnet Behaviors

Cai-Ming Liu,* De-Qing Zhang, and Dao-Ben Zhu

Beijing National Laboratory for Molecular Sciences, Center for Molecular Science, Institute of Chemistry, Chinese Academy of Sciences, Beijing 100190, People's Republic of China

Received February 19, 2009

The coordination of methanol and ethanol molecules was observed in the construction of three 1D coordination polymers composed of anti−anti carboxylato-bridged $Mn_3^{III}O(Brppz)_3$ units [Brppz = 3-(5-bromine-2-phenolate) pyrazolate]. The difference in these 1D complexes' structures induced by methanol and ethanol solvents leads to the variation of the magnetic properties. The methanol solvent product **1** $[Mn_3^{III}O(Brppz)_3(MeOH)_3(AcO)]\cdot 0.5MeOH$ has a $Mn_3^{III}O$ repeating unit with two octahedral configuration manganese(III) ions and one square-pyrimid configuration manganese(III) ion, showing a long-range magnetic ordering with a T_c of 8.2 K, whereas the ethanol solvent products **2** $[Mn_3^{III}O(Brppz)_3(C_2H_5OH)_4(AcO)]$ (α-phase) and **3** $[Mn_3^{III}O(Brppz)_3(C_2H_5OH)_4(AcO)]$ (β-phase) are polymorphs, both having a $Mn_3^{III}O$ repeating unit with three octahedral configuration manganese(III) ions, displaying single-chain magnet behaviors. Products **2** and **3** represent the first examples of polymorphs of single-chain magnets. Furthermore, the bridging carboxylate ligand in these 1D complexes was generated by the decomposition of β-diketones via the retro-Claisen condensation reactions in the presence of strong bases.

Introduction

Magnetic molecular materials have experienced great popularity in the past decades due to not only the demand to understand the essential science associated with magnetic interactions between the paramagnetic metal ions mediated by bridging ligands to develop magneto−structural correlations but also their potential applications in information storage at the molecular level and in quantum computation.[1−4] One-dimensional (1D) magnetic chain systems occupy an important position among magnetic molecular materials because many of these species were discovered to be able to exhibit not only a long-range magnetic ordering[2] but also behaviors of single-chain magnets (SCMs).[3] The latter provide the linkage between paramagnetism and long-range-ordered magnetism along with the single-molecule magnets.[4]

The magnetic properties of 1D complexes depend on both intra- and interchain interactions. For a SCM, it requires a strong and anisotropic intrachain coupling but a weak interchain coupling in order to avoid two- (2D) or three-dimensional (3D) ordering. The strong and anisotropic intrachain coupling can be realized by using anisotropic ions such as Co^{2+} and Mn^{3+} and short bridging ligands such as cyanide, azide, and carboxylate, while the interchain interaction can be weakened by bulky groups in coligands. However, because pure 1D compounds cannot create a long-range magnetic ordering at $T > 0$ K,[1a] the interchain interaction is necessary for them to exhibit the spontaneous magnetization. Therefore, it will be very interesting to investigate if the magnetic properties of a family of 1D chainlike complexes can be controlled to show a long-range magnetic ordering or behaviors of SCMs through changes of both intra- and interchain interations or not.

*To whom correspondence should be addressed. Fax: (+86)10-6256-9349. E-mail: cmliu@iccas.ac.cn.

(1) For examples: (a) Kahn, O. *Molecular Magnetism*, VCH, Weinheim, **1993**. (b) Gatteschi, D.; Kahn, O.; Miller, J. S.; Palacio, F. *Magnetic Molecular Materials*; NATO ASI, Kluwer: Dordrecht, The Netherlands, **1991**. (c) Miller, J. S.; Drillon, M. *Magnet Science: Molecules to Materials*; Wile-VCH: Weinheim, Germany, **2000**. (d) Coronado, E.; Galan-Mascaros, J. R.; Gomez-Garcia, C. J.; Laukhin, V. *Nature (London)* **2000**, *408*, 447. (e) Rikken, G. L. J. A.; Raupach, E. *Nature (London)* **2000**, *405*, 932. (f) Halder, G. J.; Kepert, C. J.; Moubaraki, B.; Murray, K. S.; Cashion, J. D. *Science* **2002**, *298*, 1762. Ohba, M.; Matsumoto, N.; Okawa, H.; Enoki, T.; Latour, J.-M. *J. Am. Chem. Soc.* **1994**, *116*, 11566. (g) Sato, O.; Tao, J.; Zhang, Y.-Z. *Angew. Chem., Int. Ed.* **2007**, *46*, 2152. (h) Ribas, J.; Escuer, A.; Monfort, M.; Vicente, R.; Cortés, R.; Lezama, L.; Rojo, T. *Coord. Chem. Rev.* **1999**, *193−195*, 1027. (i) Miller, J. S. *Adv. Mater.* **2002**, *14*, 1105. (j) Rujiwatra, A.; Kepert, C. J.; Claridge, J. B.; Rosseinsky, M. J.; Kumagai, H.; Kurmoo, M. *J. Am. Chem. Soc.* **2001**, *123*, 10584. (k) Cui, H.; Wang, Z.; Takahashi, K.; Okano, Y.; Kobayashi, H.; Kobayashi, A. *J. Am. Chem. Soc.* **2006**, *128*, 15074. (l) Gao, E.-Q.; Yue, Y.-F.; Bai, S.-Q.; He, Z.; Yan, C.-H. *J. Am. Chem. Soc.* **2004**, *126*, 1419. (m) Liu, C.-M.; Gao, S.; Zhang, D.-Q.; Huang, Y.-H.; Xiong, R.-G.; Liu, Z.-L.; Jiang, F.-C.; Zhu, D.-B. *Angew. Chem., Int. Ed.* **2004**, *43*, 990.

Published on Web 4/21/2009

Recently, the oxo-centered manganese(III) cluster unit $[Mn_3^{III}(\mu^3\text{-}O^{2-})]$, which usually results in a net magnetic moment by competing antiferromagnetic interactions, has been successfully utilized by several groups to construct 1D chainlike complexes displaying a diversity of magnetic properties.[5] For example, Sato et al. used 3-(2-phenolate)pyrazolate (ppz) and its derivative 3-(5-methyl-2-phenolate) pyrazolate (Meppz) as the coligands to generate three 1D complexes constructed from the carboxylato bridged $[Mn_3^{III}(\mu^3\text{-}O^{2-})]$ units: $[Mn_3^{III}O(ppz)_3(MeOH)_3(OAc)]$[5a] has a long-range magnetic ordering behavior, $[Mn_3^{III}O(Meppz)_3(MeOH)_4(OAc)]$[5a] shows a metamagnetic property, and $[Mn_3^{III}O(Meppz)_3(EtOH)_4(OAc)]$[5b] is a SCM with dielectric properties. Gao et al. adopted the 3,5-di-*tert*-butylsalicylaldoxime (tBu-saoH$_2$) coligand to synthesize two SCMs that are also based on the $[Mn_3^{III}(\mu^3\text{-}O^{2-})]$ units.[5c] We utilized another ppz's derivative, 3-(5-bromine-2-phenolate)pyrazolate (Brppz), as the coligand of the $[Mn_3^{III}(\mu^3\text{-}O^{2-})]$ unit and EE-azido as the bridge ligand to yield the 1D chainlike complex $[Mn_3^{III}O(Brppz)_3(MeOH)_3(N_3)]\cdot 2MeOH$,[5d] which exhibits a spin-glass behavior and a solvatomagnetic effect. To extend the work related to the $Mn_3^{III}O(Brppz)_3$ unit, systematic studies have been carried out by employing the carboxylato bridge and not only methanol but also ethanol solvents. Herein, we report the syntheses, crystal structures, and magnetic properties of three new 1D coordination polymers based on the anti−anti carboxylato bridged $[Mn_3^{III}(\mu^3\text{-}O^{2-})]$ unit and the Brppz coligand, $Mn_3^{III}O(Brppz)_3(MeOH)_3(AcO)]\cdot 0.5MeOH$ (**1**), $[Mn_3^{III}O(Brppz)_3(C_2H_5OH)_4(AcO)]$ (**2**, α-phase), and $[Mn_3^{III}O(Brppz)_3(C_2H_5OH)_4(AcO)]$ (**3**, *β*-phase). The solvents have great influence on the chain structures of these complexes, which result in quite different magnetic behaviors at low temperatures. Interestingly, **2** and **3** are polymorphs; as far as we are aware, this is the first time SCMs' polymorphs have been obtained.

Experimental Procedures

General Physical Measurements: Materials and Methods. All starting materials were commercially available and used as received without further purification. The elemental analyses were performed on a Heraeus Chn-Rapid elemental analyzer. The infrared spectra were recorded on a Pekin-Elmer 2000 spectrophotometer with pressed KBr pellets. Variable-temperature magnetic susceptibility, zero-field ac magnetic susceptibility, and field dependence of magnetization were measured on a Quantum Design MPMSXL5 (SQUID) magnetometer. Diamagnetic corrections were estimated from Pascal's constants for all constituent atoms.

Preparation of $[Mn_3^{III}O(Brppz)_3(MeOH)_3(AcO)]\cdot 0.5MeOH$ (1). Brppz (0.5 mmol) and Mn(acac)$_2$ (0.5 mmol) in 25 mL of methanol−water (v/v 10:1) mixed solvents were stirred at room temperature for 10 min; then, 0.5 mmol of NaN_3 was added. After stirring for 1 h, a dark green solution was formed, which was allowed to slowly evaporate for about two weeks, giving dark-green block crystals of **1**. Yield: 30% based on Mn. Anal. calcd for $C_{32.5}H_{32}Br_3Mn_3N_6O_{9.5}$ (**1**): C, 36.72; H, 3.03; N, 7.90. Found: C, 36.78; H, 3.08; N, 7.85. IR (KBr, cm^{-1}): 1550(m), 1482(s), 1447(m), 1398(w), 1333(w), 1290(s), 1247(w), 1144(m), 1081(m), 1021(w), 953(w), 865(w), 801(w), 775(w), 720 (m), 664(w), 620(m), 541(w), 459(w).

(2) For examples: (a) Kahn, O.; Pei, Y.; Verdaguer, M.; Renard, J. P.; Sletten, J. *J. Am. Chem. Soc.* **1988**, *110*, 782. (b) Nakatani, K.; Carriat, J. Y.; Journaux, Y.; Kahn, O.; Lloret, F.; Renard, J. P.; Pei, Y.; Sletten, J.; Verdaguer, M. *J. Am. Chem. Soc.* **1989**, *111*, 5739. (c) Pei, Y.; Kahn, O.; Nakatani, K.; Codjovi, E.; Mathonière, C.; Sletten, J. *J. Am. Chem. Soc.* **1991**, *113*, 6558. (d) Turner, S.; Kahn, O.; Rabardel, L. *J. Am. Chem. Soc.* **1996**, *118*, 6428. (e) Caneschi, A.; Gatteschi, D.; Renard, J. P.; Rey, P.; Sessoli, R. *Inorg. Chem.* **1988**, *27*, 1756. (f) Caneschi, A.; Gatteschi, D.; Renard, J. P.; Rey, P.; Sessoli, R. *Inorg. Chem.* **1989**, *28*, 1676–2940. (g) Miller, J. S.; Calabrese, J. C.; Mclean, R. S.; Epstein, A. J. *Adv. Mater.* **1992**, *4*, 498. (h) Li, L.-L.; Lin, K.-J.; Ho, C.-J.; Sun, C.-P.; Yang, H.-D. *Chem. Commun.* **2006**, 1286. (i) Miyajima, K.; Nakajima, A.; Yabushita, S.; Knickelbein, M. B.; Kaya, K. *J. Am. Chem. Soc.* **2004**, *126*, 13202. (j) Yuan, M.; Zhao, F.; Zhang, W.; Pan, F.; Wang, Z.-M.; Gao, S. *Chem.—Eur. J.* **2007**, *13*, 2937.

(3) For examples: (a) Clérac, R.; Miyasaka, H.; Yamashita, M.; Coulon, M. C. *J. Am. Chem. Soc.* **2002**, *124*, 12837. (b) Wang, S.; Zuo, J.-L.; Gao, S.; Song, Y.; Zhou, H.-C.; Zhang, Y.-Z.; You, X.-Z. *J. Am. Chem. Soc.* **2004**, *126*, 8900. (c) Bogani, L.; Sangregorio, C.; Sessoli, R.; Gatteschi, D. *Angew. Chem., Int. Ed.* **2005**, *44*, 5817. (d) Pardo, E.; Ruiz-García, R.; Lloret, F.; Faus, J.; Julve, M.; Journaux, Y.; Delgado, F.; Ruiz-Pérez, C. *Adv. Mater.* **2004**, *16*, 1597. (e) Ferbinteanu, M.; Miyasaka, H.; Wernsdorfer, W.; Nakata, K.; Sugiura, K.; Yamashita, M.; Coulon, C.; Clérac, R. *J. Am. Chem. Soc.* **2005**, *127*, 3090. (f) Toma, L. M.; Lescouëzec, R.; Pasán, J.; Ruiz-Pérez, C.; Vaissermann, J.; Cano, J.; Carrasco, R.; Wernsdorfer, W.; Lloret, F.; Julve, M. *J. Am. Chem. Soc.* **2006**, *128*, 4842. (g) Liu, T.-F.; Fu, D.; Gao, S.; Zhang, Y.-Z.; Sun, H.-L.; Su, G.; Liu, Y.-J. *J. Am. Chem. Soc.* **2003**, *125*, 13976. (h) Zhang, X.-M.; Hao, Z.-M.; Zhang, W.-X.; Chen, X.-M. *Angew. Chem., Int. Ed.* **2007**, *46*, 3456. (i) Miyasaka, H.; Madanbashi, T.; Sugimoto, K.; Nakazawa, Y.; Wernsdorfer, W.; Sugiura, K.; Yamashita, M.; Coulon, C.; Clérac, R. *Chem.—Eur. J.* **2006**, *12*, 7028. (j) Palii, A. V.; Reu, O. S.; Ostrovsky, S. M.; Klokishner, S. I.; Tsukerblat, B. S.; Sun, Z.-M.; Mao J.-G.; Prosvirin, A. V.; Zhao, H.-H.; Dunbar, K. R. *J. Am. Chem. Soc.* **2008**, *130*, 14729. (k) Stamatatos, T. C.; Abboud, K. A.; Wernsdorfer, W.; Christou, G. *Inorg. Chem.* **2009**, *48*, 807. (l) Choi, S. W.; Kwak, H. Y.; Yoon, J. H.; Kim, H. C.; Koh, E. K.; Hong, C. S. *Inorg. Chem.* **2008**, *47*, 10214. (m) Zheng, Y.-Z.; Xue, W.; Tong, M.-L.; Chen, X.-M.; Zheng, S.-L. *Inorg. Chem.* **2008**, *47*, 11202. (n) Bernot, K.; Luzon, J.; Sessoli, R.; Vindigni, A.; Thion, J.; Richeter, S.; Leclercq, D.; Larionova, J.; van der Lee, A. *J. Am. Chem. Soc.* **2008**, *130*, 1619. (o) Chakov, N. E.; Wernsdorfer, W.; Abboud, K. A.; Christou, G. *Inorg. Chem.* **2004**, *43*, 5919. (p) Zheng, Y.-Z.; Tong, M.-L.; Zhang, W.-X.; Chen, X.-M. *Angew. Chem., Int. Ed.* **2006**, *45*, 6310. (q) Brockman, J. T.; Stamatatos, Th. C.; Wernsdorfer, W.; Abboud, K. A.; Christou, G. *Inorg. Chem.* **2007**, *46*, 9160. (r) Coulon, C.; Miyasaka, H.; Clérac, R. *Struct. Bonding (Berlin)* **2006**, *122*, 163.

(4) For examples: (a) Sessoli, R.; Gatteschi, D.; Caneschi, A.; Novak, M. A. *Nature (London)* **1993**, *365*, 141. (b) Gatteschi, D.; Sessoli, R. *Angew. Chem., Int. Ed.* **2003**, *42*, 268. (c) Wernsdorfer, W.; Aliaga-Alcalde, N.; Hendrickson, D. N.; Christou, G. *Nature (London)* **2002**, *416*, 406. (d) Sessoli, R.; Tsai, H. L.; Schake, A. R.; Wang, S.; Vincent, J. B.; Folting, K.; Gatteschi, D.; Christou, G.; Hendrickson, D. N. *J. Am. Chem. Soc.* **1993**, *115*, 1804. (e) Ruiz, D.; Sun, Z.; Albela, B.; Folting, K.; Christou, G.; Hendrickson, D. N. *Angew. Chem., Int. Ed.* **1998**, *37*, 300. (f) Song, Y.; Zhang, P.; Ren, X.-M.; Shen, X.-F.; Li, Y.-Z.; You, X.-Z. *J. Am. Chem. Soc.* **2005**, *127*, 3708. (g) Ni, Z.-H.; Kou, H.-Z.; Zhang, L.-F.; Ge, C.; Cui, A.-L.; Wang, R.-J.; Li, Y.-D.; Sato, O. *Angew. Chem., Int. Ed.* **2005**, *44*, 7742. (h) Oshio, H.; Nihei, M.; Yoshida, A.; Nojiri, H.; Nakano, M.; Yamaguchi, A.; Karaki, Y.; Ishimoto, H. *Chem.—Eur. J.* **2005**, *11*, 843. (i) Schelter, E. J.; Prosvirin, A. V.; Dunbar, K. R. *J. Am. Chem. Soc.* **2004**, *126*, 15004. (j) Freedman, D. E.; Jenkins, D. M.; Iavarone, A. T.; Long, J. R. *J. Am. Chem. Soc.* **2008**, *130*, 2884. (k) Ma, Y.-S.; Li, Y.-Z.; Song, Y.; Zheng, L.-M. *Inorg. Chem.* **2008**, *47*, 4536. (l) Stamatatos, T. C.; Nastopoulos, V.; Tasiopoulos, A. J.; Moushi, E. E.; Wernsdorfer, W.; Christou, G.; Perlepes, S. P. *Inorg. Chem.* **2008**, *47*, 10081. (m) Stamatatos, T. C.; Poole, K. M.; Abboud, K. A.; Wernsdorfer, W.; O'Brien, T. A.; Christou, G. *Inorg. Chem.* **2008**, *47*, 5006. (n) Milios, C. J.; Inglis, R.; Vinslava, A.; Bagai, R.; Wernsdorfer, W.; Parsons, S.; Perlepes, S. P.; Christou, G.; Brechin, E. K. *J. Am. Chem. Soc.* **2007**, *129*, 12505. (o) Hiraga, H.; Miyasaka, H.; Nakata, K.; Kajiwara, T.; Takaishi, S.; Oshima, Y.; Nojiri, H.; Yamashita, M. *Inorg. Chem.* **2007**, *46*, 9661. (p) Glaser, T.; Heidemeier, M.; Weyhermüller, T.; Hoffmann, R.-D.; Rupp, H.; Müller, P. *Angew. Chem., Int. Ed.* **2006**, *45*, 6033. (q) Chandrasekhar, V.; Pandian, B. M.; Vittal, J. J.; Clérac, R. *Inorg. Chem.* **2009**, *48*, 1148. (r) Aromi, G.; Brechin, E. K. *Struct. Bonding (Berlin)* **2006**, *122*, 1.

(5) (a) Tao, J.; Zhang, Y.-Z.; Bai, Y.-L.; Sato, O. *Inorg. Chem.* **2006**, *45*, 4877. (b) Bai, Y.-L.; Tao, J.; Wernsdorfer, W.; Sato, O.; Huang, R.-B.; Zheng, L.-S. *J. Am. Chem. Soc.* **2006**, *128*, 16428. (c) Xu, H.-B.; Wang B.-W.; Pan, H.; Wang, Z.-M.; Gao, S. *Angew. Chem., Int. Ed.* **2007**, *46*, 7388. (d) Liu, C.-M.; Zhang, D.-Q.; Zhu, D.-B. *Chem. Commun.* **2008**, 368. (e) Kim, J.; Lim, J. M.; Do, Y. *Eur. J. Inorg. Chem.* **2003**, 2563.

Preparation of $[Mn_3^{III}O(Brppz)_3(C_2H_5OH)_3(AcO)]$ (2). Brppz (0.5 mmol), $Mn(acac)_2$ (0.5 mmol), $Gd(NO_3)_3\cdot 6H_2O$ (0.1 mmol), and NaN_3 (1.0 mmol) in 44 mL of ethanol−water (v/v 10:1) mixed solvents were stirred at room temperature for 6 h and filtered. The dark green filtrate was allowed to slowly evaporate for about two weeks, giving dark-green lathy crystals of **2**. Yield: 32% based on Mn. Anal. calcd for $C_{37}H_{42}Br_3Mn_3N_6O_{10}$ (**2**): C, 39.14; H, 3.73; N, 7.40. Found: C, 39.12; H, 3.79; N, 7.35. IR (KBr, cm^{-1}): 1567(m), 1482(s), 1447(m), 1399(w), 1333(w), 1289(s), 1246(w), 1144(m), 1081(m), 864(w), 810(w), 776(w), 720(m), 665(w), 621(m), 459(w).

Preparation of $[Mn_3^{III}O(Brppz)_3(C_2H_5OH)_3(AcO)]$ (3). Brppz (0.5 mmol), $Mn(acac)_2$ (0.5 mmol), and NaN_3 (1.0 mmol) in 44 mL of ethanol−water (v/v 10:1) mixed solvents were stirred at room temperature for 6 h and filtered. Black block crystals grew from the filtrate after one month. Yield: 45% based on Mn. Anal. calcd for $C_{37}H_{42}Br_3Mn_3N_6O_{10}$ (**3**): C, 39.14; H, 3.73; N, 7.40. Found: C, 39.17; H, 3.78; N, 7.36. IR(KBr, cm^{-1}): 1550 (m), 1482(s), 1447(m), 1397(w), 1334(w), 1288(s), 1246(w), 1146 (m), 1080(m), 953(w), 864(w), 814(w), 777(w), 719(s), 665(w), 619(m), 456(w).

Structure Determination. The data were collected on a Rigaku RAXIS RAPID IP imaging plate system (for **1** and **2**) or Bruker SMART APEX-CCD diffractometer (for **3**) with Mo Ka radiation (λ = 0.71073 Å). The structures were solved by direct methods and refined by the full-matrix least-squares technique on F^2 using the SHELXL97 program. All non-hydrogen atoms were refined anisotropically. Hydrogen atoms defined by the stereochemistry were placed at their calculated positions and allowed to ride on their host carbon atoms. Crystallographic data are listed in Table 1 and selected bond lengths and angles in Table 2.

Result and Discussion

Synthesis. Complexes **1**−**3** were all obtained through "one-pot" preparation and by the method of solvent evaporation. $MnCl_2$, $Mn(CH_3CO_3)_2$, and $Mn(HCO_3)_2$ have been successfully used as the manganese sources to synthesize several 1D coordination polymers constructed from the $Mn_3^{III}O$ units by Sato's and Gao's groups,[5a−c] while we found that $Mn(acac)_2$ is also a good manganese source to generate the $Mn_3^{III}O$ units.[5d] Sodium azide was utilized to act as a base. Though no acetate-based Mn starting material was utilized to prepare **1**−**3**, the acetate anion was generated to bridge the $Mn_3^{III}O$ units in these complexes. Obviously, this bridging ligand is one of the decomposition products of the $acac^-$ ligand. β-Diketones have been known to be able to undergo the retro-Claisen condensation reaction to produce a ketone and a carboxylate when strong bases are present.[6] In addition, the lanthanide salt $Gd(NO_3)_3\cdot 6H_2O$ seems to be able to stay the decomposition of $acac^-$ into $CH_3CO_3^-$ to some degree, as indicated by the preparation of $[Mn_3^{III}O(Brppz)_3(MeOH)_3(N_3)]\cdot 2MeOH$.[5d] It was found that under similar reaction conditions azido-bridged complex $[Mn_3^{III}O(Brppz)_3(MeOH)_3(N_3)]\cdot 2MeOH$ was more easily formed than the carboxylato-bridged complex **1** in the presence of $Gd(NO_3)_3\cdot 6H_2O$. However, such a stay role can be overcome by a longer reaction time; for example, the carboxylato-bridged complex **2** was also generated, even in the presence of $Gd(NO_3)_3\cdot 6H_2O$, when more reaction time was used with respect to $[Mn_3^{III}O(Brppz)_3(MeOH)_3(N_3)]\cdot 2MeOH$.[5d] Very interestingly, different polymorphs of $[Mn_3^{III}O(Brppz)_3(C_2H_5OH)_4(AcO)]$ were obtained in the presence of $Gd(NO_3)_3\cdot 6H_2O$ (for **2**) or without $Gd(NO_3)_3\cdot 6H_2O$ (for **3**), suggesting that $Gd(NO_3)_3\cdot 6H_2O$ can change the approach to the formation of $[Mn_3^{III}O(Brppz)_3(C_2H_5OH)_4(AcO)]$ effectively.

Crystal Structures. The manganese oxidation states were established by bond-valence sum (BVS) calculations.[7] Both **2** and **3** are thermally stable; it seems that the two polymorphs cannot transform each other by a change of temperatures because each of them maintains the same crystal cell either at room temperature or at temperatures as low as 173 K.

Complex 1. Single-crystal X-ray analysis revealed that **1** has a similar structure to that of $[Mn_3^{III}O(Brppz)_3(MeOH)_3(N_3)]\cdot 2MeOH$,[5d] except for the anti−anti carboxylato bridge instead of the EE-azido bridge. As shown in Figure 1, complex **1** features an anti−anti carboxylato-bridged trinuclear-$Mn_3^{III}O$-based chain. The edge of the triangular unit $[Mn_3^{III}(\mu^3\text{-}O^{2-})]$ is bridged by the $\eta^1/\eta^1/\mu$-pyrazole group of the Brppz coligand, whose η^1-phenolate group coordinates to the vertex manganese atom. Similar cases were also observed in quite recently reported $[Mn_3^{III}O(Brppz)_3(MeOH)_3(N_3)]\cdot 2MeOH$,[5d] $[Mn_3^{III}O(Meppz)_3(EtOH)_4(OAc)]$,[5b] $[Mn_3^{III}O(Meppz)_3\text{-}(MeOH)_4(OAc)]$,[5a] and $[Mn_3^{III}O(ppz)_3(MeOH)_3(OAc)]$.[5a] The central oxygen atom locates 0.0279 Å above the $Mn_3^{III}O$ plane. The average intracluster Mn···Mn separation of 3.302 Å is a little shorter than that in $[Mn_3^{III}O\text{-}(Brppz)_3(MeOH)_3(N_3)]\cdot 2MeOH$ (3.323 Å),[5d] but slightly longer than that of $[Mn_3^{III}O(ppz)_3(MeOH)_3(OAc)]$ (3.295 Å).[5a]

There are three crystallographically independent manganese atoms in the $[Mn_3^{III}(\mu^3\text{-}O^{2-})]$ unit. Either the Mn1 atom or Mn2 atom adopts a distorted octahedral geometry, with a similar basal plane $[N_2O_2]$ composed of the central $\mu^3\text{-}O^{2-}$ ion, one N atom and one phenolate O atom from one Brppz coligand, and one N atom from another Brppz coligand. However, one carboxylato O atom and one O atom of one ethanol molecule occupy the apical positions of Mn1, while another two methanol ligands are situated at two apical positions of Mn2. Quite differently, Mn3 exhibits a distorted square-pyrimid configuration, which shows a similar basal plane $[N_2O_2]$ to those of Mn1 and Mn2, but a carboxylato O atom occupying the only apical site of the square pyrimid. For the octahedral configuration Mn1 and Mn2 ions, the $Mn-O_{apiçal}$ distances [2.302(3)−2.363(3) and 2.271 (3)−2.275(3) Å for Mn1 and Mn2, respectively] are obviously longer than the $Mn-O_{equatorial}$ and $Mn-N_{equatorial}$ bond distances [1.854(3)−1.998(3) and 1.855(2)−2.002(3) for Mn1 and Mn2, respectively], which means that the two Mn^{3+} ions display a classical Jahn−Teller (JT) elongation, as expected for the high-spin $3d^4$ Mn^{III} ion. In addition, the apical axes of all three Mn^{3+} ions are

(6) (a) Milios, C. J.; Kyritsis, P.; Raptopoulou, C. P.; Terzis, A.; Vicente, R.; Escuer, A.; Perlepes, S. P. *Dalton Trans* **2005**, 501. (b) Wang, S.; Pang, Z.; Smith, K. D. L.; Hua, Y.-S.; Deslippe, C.; Wagner, M. J. *Inorg. Chem.* **1995**, *34*, 908. (c) Drake, S. R.; Lyons, A.; Otway, D. J.; Williams, D. J. *Inorg. Chem.* **1994**, *33*, 1230. (d) Milios, C. J.; Kefalloniti, E.; Raptopoulou, C. P.; Terzis, A.; Escuer, A.; Vicente, R.; Perlepes, S. P. *Polyhedron* **2004**, *23*, 83. (e) Liu, C.-M.; Zhang, D.-Q.; Zhu, D.-B. *Inorg. Chem.* **2009**, *48*, 792.

(7) (a) Liu, W.; Thorp, H. H. *Inorg. Chem.* **1993**, *32*, 4102. (b) BVS for **1**: Mn1, Mn2, and Mn3 are 3.13, 3.17, and 3.08, respectively. For **2**: Mn1, Mn2, and Mn3 are 3.07, 3.02, and 3.05, respectively. For **3**: Mn1, Mn2, and Mn3 are 3.20, 3.22, and 3.21, respectively.

Table 1. Crystal Data and Structural Refinement Parameters for **1**−**3**

	1	**2**	**3**
formula	$C_{32.5}H_{32}Br_3Mn_3N_6O_{9.5}$	$C_{37}H_{42}Br_3Mn_3N_6O_{10}$	$C_{37}H_{42}Br_3Mn_3N_6O_{10}$
fw	1063.19	1135.32	1135.32
cryst syst	monoclinic	orthorhombic	monoclinic
space group	$P2_1/c$	$P2_12_12_1$	$P2_1/c$
a [Å]	7.604(2)	7.789(2)	7.820(2)
b [Å]	33.436(7)	17.352(3)	42.017(8)
c [Å]	15.726(3)	31.176(6)	13.568(3)
β [deg]	91.95(3)	90	100.08(3)
V [Å^3]	3996.0(15)	4213.6(15)	4389.3(17)
Z	4	4	4
ρ_{calcd} [g cm^{-3}]	1.767	1.790	1.718
μ [mm^{-1}]	3.992	3.793	3.641
T [K]	293(2)	173(2)	293(2)
λ(Mo Kα) [Å]	0.71073	0.71073	0.71073
reflns collected	21934	22518	24713
unique reflns	7001	7429	7717
observed reflns	5160	6754	5949
params	2100	2264	2264
GoF	1.169	1.123	1.022
R_1[a]	0.0942	0.0776	0.0444
wR_2[b]	0.1805	0.1739	0.1064

[a] $R_1 = \sum||F_o| - |F_c||/\sum|F_o|$. [b] $wR_2 = \sum\{[w(F_o^2 - F_c^2)^2]/\sum[wF_o^2]^2\}^1$.

nearly parallel to each other and are roughly perpendicular to the $Mn_3^{III}O$ plane.

Each $Mn_3^{III}O$ unit is connected with adjacent ones by using the acetate groups as bridges in the anti−anti coordination mode, forming a 1D stepwise chain structure along the *a* axis. The acetato-bridged Mn···Mn distance in **1** is 6.50 Å, a little longer than that of $[Mn_3^{III}O(Meppz)_3(MeOH)_3(OAc)]$ (6.39 Å).[5b] Furthermore, neighboring 1D chains are connected with each other through the Mn···Br short-contact weak interaction, with a Mn···Br distance of 3.351 Å, generating a ruffling supramolecular layer along the *ac* plane, with a period of 15.726(3) Å (the length of the *c* axis; Figure 1b). Such an intermolecular weak interaction not only plays an important role in stabilization of the crystal structure of **1** but also favors its long-range magnetic ordering, which will be discussed in the Magnetic Properties section. For comparison, the dimerlike double chain structures are formed in $[Mn_3^{III}O(Brppz)_3(MeOH)_3(N_3)]\cdot 2MeOH$[5d] through the Mn···Br short contact weak interaction between two neighboring 1D chains, with a Mn···Br distance of 3.641 Å that is obviously larger than that of **1** (3.351 Å). The interchain distance separated by the nearest central oxygen atoms of the Mn_3O units within the supramolecular layer of **1** is 11.782 Å, longer than that between the supramolecular layers (10.831 Å).

Complexes 2 and 3. Both **2** and **3** have similar structures to that of **1**, except that all three manganese atoms in the $[Mn_3^{III}(\mu^3\text{-}O^{2-})]$ unit of **2** and **3** rather than only two manganese atoms in the $[Mn_3^{III}(\mu^3\text{-}O^{2-})]$ unit of **1** are six-coordinated, and the coordination ethanol molecules in **2** and **3** take the place of the coordination methanol ligands in **1** (Figures 2 and 3). Complexes **2** and **3** are polymorphs. However, **2** crystallizes in chiral space group $P2_12_12_1$, whereas **3** crystallizes in the centrosymmetric $P2_1/c$. Similar to **1**, one μ^3-O^{2-} center atom bridges three manganese(III) atoms to generate the nearly planar triangular cluster unit $Mn_3^{III}O$. The central oxygen atoms locate 0.0016 Å above the $Mn_3^{III}O$ plane for **2** but −0.0240 Å below the Mn_3^{III} plane for **3**. And the average intracluster Mn···Mn separation of 3.305 Å in **2** is comparable with that in **1** (3.302 Å) but slightly longer than that in **3** (3.295 Å).

Like **1**, there are three crystallographically independent manganese atoms in either **2** or **3**. Each Mn atom in both complexes adopts a distorted octahedral geometry, with a similar basal plane $[N_2O_2]$ to that of **1**. However, one carboxylato O atom and one O atom of an ethanol molecule occupy the apical positions of Mn1 and Mn2, while two ethanol ligands are situated at two apical positions of Mn3. The JT elongation of the Mn^{III} ions in both **2** and **3** is also remarkable: the $Mn-O_{apical}$ distances in **2** [2.290(7)−2.300(8), 2.310(6)−2.310(7), and 2.323(8)−2.356(6) Å for Mn1, Mn2, and Mn3, respectively] are longer than the $Mn-O_{equatorial}$ and $Mn-N_{equatorial}$ bond lengths [1.852(6)−2.018(8), 1.862(7)−1.989(7), and 1.843(5)−1.996(8) Å for Mn1, Mn2, and Mn3, respectively], and the $Mn-O_{apical}$ distances in **3** [2.302(3)−2.340(3), 2.343(3)−2.344(3), and 2.270(3)−2.348(3) Å for Mn1, Mn2, and Mn3, respectively] are longer than the $Mn-O_{equatorial}$ and $Mn-N_{equatorial}$ bond lengths [1.846(3)−1.993(3), 1.847(3)−1.986(3), and 1.848(3)−2.006(3) Å for Mn1, Mn2, and Mn3, respectively]. Similar to **1**, the JT axes of all three Mn^{3+} ions in both **2** and **3** are almost parallel to each other and are approximately perpendicular to the $Mn_3^{III}O$ plane.

The $Mn_3^{III}O$ units link to each other through the carboxylato bridges in the anti−anti coordination mode to generate 1D stepwise chains for **2** (Figure 2b) and **3** (Figure 3b). The Mn···Mn separation through the carboxylato bridge in **2** is 6.713 Å, slightly longer than those in **3** (6.690 Å), **1** (6.50 Å), and $[Mn_3^{III}O(Meppz)_3(EtOH)_4(OAc)]$ (6.606 Å).[5b] All Mn_3O planes in the same chain are parallel to each other, and the chains run parallel to the *a*-axis direction in both complexes **2** and **3** (Figures 2b and 3b). Differently, there are four planes (5 3 11), (5 −3 11), (−5 3 11), and (−5 −3 11) in **2** but only two planes (7 23 −3) and (−7 23 3) in **3** to which the Mn_3O planes from different chains are parallel. And the interchain distances separated by the nearest central oxygen atoms of the Mn_3O units in **2**

Table 2. Selected Bond Lengths (Å) and Angles (deg) of **1**−**3**

1 (#1: $x + 1, y, z$; #2: $x - 1, y, z$)

Mn1−O1	1.854(3)	Mn1−O4	1.906(2)
Mn1−N1	1.946(3)	Mn1−N4	1.998(3)
Mn1−O5	2.302(3)	Mn1−O7	2.363(3)
Mn2−O2	1.855(2)	Mn2−O4	1.905(2)
Mn2−N3	1.957(3)	Mn2−N6	2.002(3)
Mn2−O9	2.271(3)	Mn2−O8	2.275(3)
Mn3−O3	1.850(3)	Mn3−O4	1.908(2)
Mn3−N5	1.951(3)	Mn3−N2	1.980(3)
Mn3−O6#1	2.156(3)	O6−Mn3#2	2.156(3)
O1−Mn1−O4	179.58(10)	N1−Mn1−N4	177.07(13)
O5−Mn1−O7	168.33(11)	O2−Mn2−O4	178.60(11)
N3−Mn2−N6	176.98(13)	O9−Mn2−O8	174.35(10)
O3−Mn3−O4	173.37(11)	N5−Mn3−N2	161.53(12)
Mn2−O4−Mn1	120.56(11)	Mn2−O4−Mn3	119.18(11)
Mn1−O4−Mn3	120.20(11)		

2 (#1: $x + 1, y, z$)

Mn2−O3	1.862(7)	Mn2−O4	1.917(6)
Mn2−N5	1.962(7)	Mn2−N4	1.989(7)
Mn2−O10#1	2.310(6)	Mn2−O9	2.310(7)
Mn1−O2	1.852(6)	Mn1−O4	1.907(5)
Mn1−N3	1.973(8)	Mn1−N2	2.018(8)
Mn1−O7	2.290(7)	Mn1−O8	2.300(8)
Mn3−O1	1.843(5)	Mn3−O4	1.900(5)
Mn3−N1	1.977(8)	Mn3−N6	1.996(8)
Mn3−O6	2.323(8)	Mn3−O5	2.356(6)
O3−Mn2−O4	178.9(3)	N5−Mn2−N4	177.4(3)
O10#1−Mn2-O9	172.4(3)	O2−Mn1−O4	177.4(3)
N3−Mn1−N2	173.0(3)	O7−Mn1−O8	165.8(3)
O1−Mn3−O4	176.2(3)	N1−Mn3−N6	177.7(3)
O6−Mn3−O5	163.3(3)	Mn3−O4−Mn1	120.4(3)
Mn3−O4−Mn2	119.3(3)	Mn1−O4−Mn2	120.3(3)

3 (#1: $x + 1, y, z$)

Mn1−O2	1.846(3)	Mn1−O1	1.911(2)
Mn1−N1	1.947(3)	Mn1−N6	1.993(3)
Mn1−O7	2.302(3)	Mn1−O5	2.340(3)
Mn2−O3	1.847(3)	Mn2−O1	1.894(2)
Mn2−N3	1.958(3)	Mn2−N2	1.986(3)
Mn2−O10	2.343(3)	Mn2−O6#1	2.344(3)
Mn3−O4	1.848(3)	Mn3−O1	1.903(2)
Mn3−N5	1.951(3)	Mn3−N4	2.006(3)
Mn3−O8	2.270(3)	Mn3−O9	2.348(3)
O2−Mn1−O1	179.35(14)	N1−Mn1−N6	174.43(14)
O7−Mn1−O5	170.48(12)	O3−Mn2−O1	178.82(13)
N3−Mn2−N2	176.92(14)	O10−Mn2−O6#1	170.27(12)
O4−Mn3−O1	179.34(14)	N5−Mn3−N4	178.37(14)
O8−Mn3−O9	171.81(12)	Mn2−O1−Mn3	120.15(13)
Mn2−O1−Mn1	119.54(13)	Mn3−O1−Mn1	120.22(13)

are 11.100 and 11.128 Å, smaller than those of **3** (11.865 and 13.264 Å), indicating a better isolation of the chains in **3** with respect to **2**. Instead of the Mn···Br short contact weak interchain interaction in **1**, the chains of **2** and **3** are stabilized by the intramolecular hydrogen bonds: there are two hydrogen bonds between the oxygen atoms of the acetate groups and the coordinated ethanol molecules [O5···O7, 2.706(9) Å; O6···O10$^{\#1}$, 2.704(11) Å, $^{\#1}$ $x + 1, y, z$] and one hydrogen bond between the coordinated ethanol molecules [O5···O9, 2.917(10) Å] in **2** and there are three hydrogen bonds between the oxygen atoms of acetate groups and the coordinated ethanol molecules [O7···O6$^{\#1}$, 3.024(5) Å; O8···O6$^{\#1}$, 2.688(4) Å; and O5···O9, 2.766(5) Å, $^{\#1}$ $x + 1, y, z$] in **3**. Similar intramolecular hydrogen bonds were also observed in [Mn_3^{III}O(Meppz)$_3$(MeOH)$_4$(OAc)][5a] and [Mn_3^{III}O(ppz)$_3$(MeOH)$_3$(OAc)].[5a]

Magnetic Properties. Complex 1. The thermal variation χT for **1** under a 1 kOe applied field is shown in Figure 4a. The value of χT at room temperature of **1** (8.33 emu·K·mol^{-1}) is a little smaller than the spin-only value for three noninteracting manganese(III) ions (9.00 emu·K·mol^{-1} for $g = 2.0$). The χT product in **1** decreases continuously and falls rapidly when $T < 100$ K upon cooling, suggesting dominant intracluster antiferromagnetic interactions. χT reaches a minimum 3.12 emu·K·mol^{-1} at 18 K, then increases to a maximum at 7 K, with a value of 38.02 emu·K·mol^{-1}, and then falls, which may arise from zero-field splitting, Zeeman effects, or weak interchain interactions.

The susceptibility data of **1** above 30 K follow the Curie−Weiss law, with $C = 9.65$ cm^3 mol^{-1} K and $\Theta = -47.24$ K. The magnetic susceptibility data of **1** were fitted to the theoretical expression for an isosceles triangle (J_1, J_2)

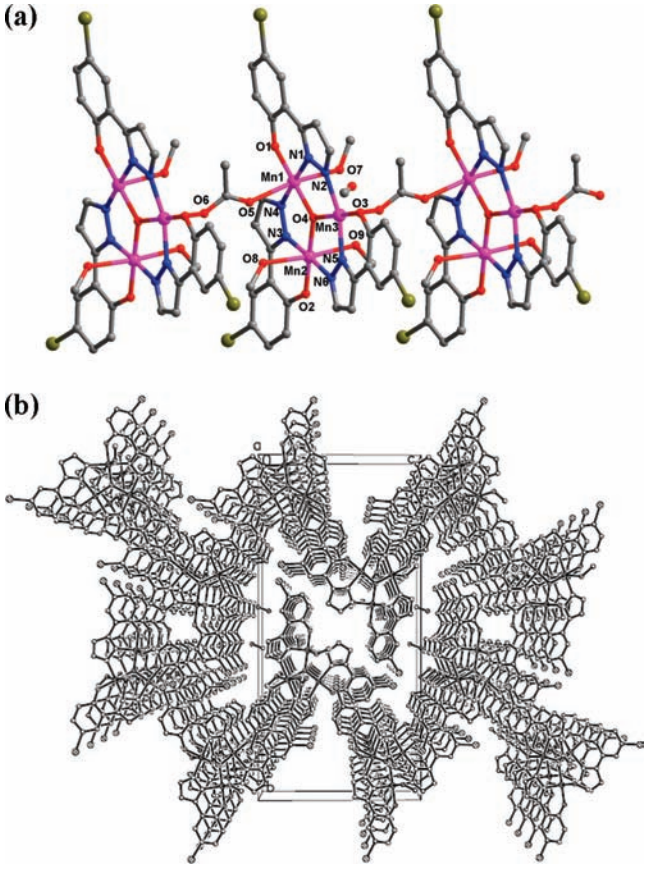

Figure 1. 1D chainlike structure of **1** (a) and projection down the *a* axis of **1**, showing Mn···Br short contacts, generating an interesting two-dimensional supramolecular array along the *ac* plane (b).

model [$H = -2J_1(\sum S_1S_2 + \sum S_1S_3) - 2J_2 \sum S_2S_3$, with $S_1 = S_2 = S_3 = 2$] above 20 K by treating the intrachain interunit interactions with mean-field approximations (zJ),[5b] giving $J_1 = -1.58$ cm^{-1}, $J_2 = -5.50$ cm^{-1}, $g = 2.04$, and $zJ = -0.27$ cm^{-1} with $R = 3.7 \times 10^{-4}$. The negative zJ value indicates weak antiferromagnetic interactions via the anti−anti carboxylato bridges, as observed in $[Mn_3^{III}O(Meppz)_3(EtOH)_4(OAc)]$,[5b] but is completely different from that in the analogues with the ppz and Meppz coligands, $[Mn_3^{III}O(Meppz)_3(MeOH)_4(OAc)]$[5a] and $[Mn_3^{III}O(ppz)_3(MeOH)_3(OAc)]$,[5a] whose anti−anti carboxylato bridges mediate ferromagnetic interactions.

A weak ferromagnetism probably arising from spin canting was observed. The divergence of the zero-field-cooled (ZFC) and field-cooled (FC) susceptibilities below about 8 K suggests an irreversible behavior of long-range magnetic ordering (Figure 4b). The ac susceptibility measurements indicate that both $\chi_{ac}'(T)$ and $\chi_{ac}''(T)$ are frequency-independent (Figure 4c and d), excluding any glassy or superparamagnetic behaviors. Both $\chi_{ac}'(T)$ and $\chi_{ac}''(T)$ curves show that the transition temperature is 8.2 K, and a nonzero $\chi_{ac}''(T)$ component suggests hysteretic effects and an uncompensated moment. Isothermal magnetization experiments performed at 2 K exhibit a hysteresis with a large coercive field of 5028 Oe and a remnant magnetization of 1.38 emu·Oe·mol^{-1} (Figure 4e). As shown in Figure 4f, the $M-H$ curve of **1** measured at 2 K shows a sigmoidal shape, suggesting a spin-flop transition[1m] when the field is large enough (about

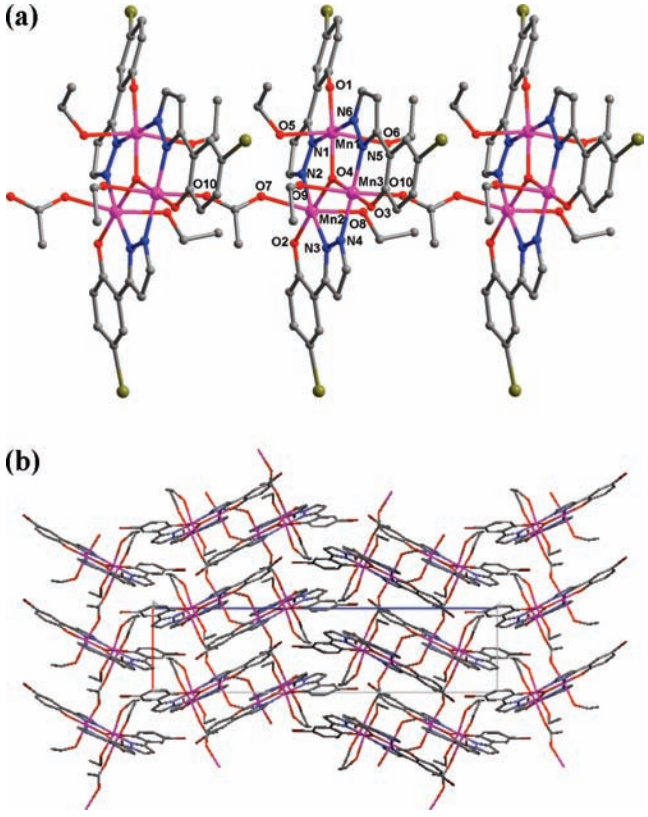

Figure 2. 1D chain structure of **2** (a) and packing diagram of **2** viewed down the *b* axis (b).

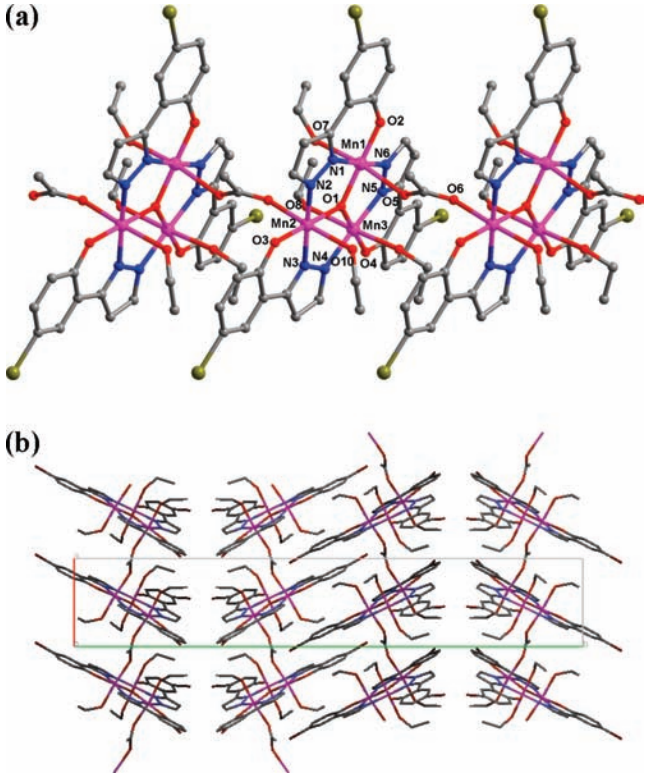

Figure 3. 1D chain structure of **3** (a) and view of the packing arrangement of **3** down the *c* axis (b).

3500 G), which happens if the Ising-like anisotropy is small with respect to the weakest antiferromagnetic interaction. The M value at 5 T is only 2.67 Nβ, far from the saturation

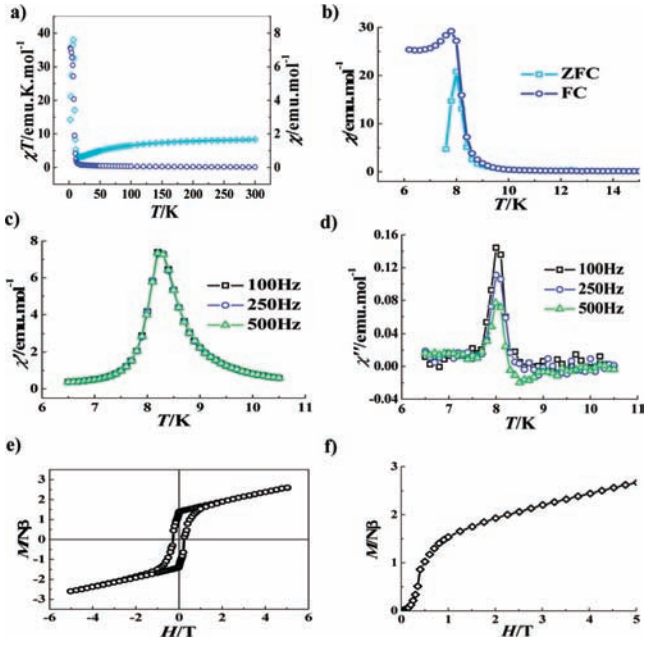

Figure 4. Plots of χT (cyan) and χ (blue) versus T of **1** measured under 1 kOe (a). The solid lines represent the best theoretical fitting. Plots of field-cooled (FC) and zero-field-cooled (ZFC) susceptibility for **1** (b). Real χ' ac magnetic susceptibility as a function of temperature at different frequencies for **1** (c). Imaginary χ'' ac magnetic susceptibility as a function of the temperature at different frequencies for **1** (d). The hysteresis loop at 2 K for **1** (e). M−H curve at 2 K for **1** (f).

value of 12 Nβ expected for a trinuclear [Mn_3^{III}] system, which is consistent with the weak ferromagnetism owing to spin canting. Because a pure 1D system cannot create long-range magnetic ordering at $T > 0$ K,[1a] the interchain Mn···Br short contact weak interactions in **1** play an important role in its showing a long-range magnetic ordering through forming a 2D supramolecular array. A long-range magnetic ordering was also observed in [$Mn_3^{III}O(ppz)_3(MeOH)_3(OAc)$],[5a] but its Tc value of 3.2 K is much lower than that in **1** (8.2 K) and its coercive field is much smaller with respect to **1**.

Complexes 2 and 3. The thermal variation χT for **2** under a 1 kOe applied field in the temperature range of 2−300 K is shown in Figure 5a. The value of χT at room temperature is 8.33 emu·K·mol^{-1}, somewhat smaller than the 9.00 emu·K·mol^{-1} spin-only value ($g = 2.0$) expected for a Mn_3^{III} complex with noninteracting metal centers. The χT product decreases continuously and falls rapidly when $T < 100$ K upon cooling, reaching a minimum at 15 K, and then increases abruptly to a maximum at 4 K with a value of 12.58 emu·K·mol^{-1}, suggesting a canted antiferromagnetic-like character.[5c] The χT value falling below 4 K may arise from zero-field splitting, Zeeman effects, or weak interchain interactions too.

The susceptibility data of **2** above 25 K obey the Curie−Weiss law, with $C = 9.38$ cm^3 mol^{-1} K and $\Theta = -35.60$ K. The least-squares fitting of the experimental χT vs T data above 16 K with the same theoretical expression for an isosceles triangle (J_1, J_2) model as utilized for **1**[5b] gives $J_1 = -1.02$ cm^{-1}, $J_2 = -4.39$ cm^{-1}, $zJ = -0.31$ cm^{-1}, and $g = 2.02$ with $R = 4.12 \times 10^{-4}$. The small negative zJ value corresponds to weak antiferromagnetic interactions via anti−anti carboxylato bridges, as observed in **1** and [$Mn_3^{III}O(Meppz)_3(EtOH)_4(OAc)$].[5b]

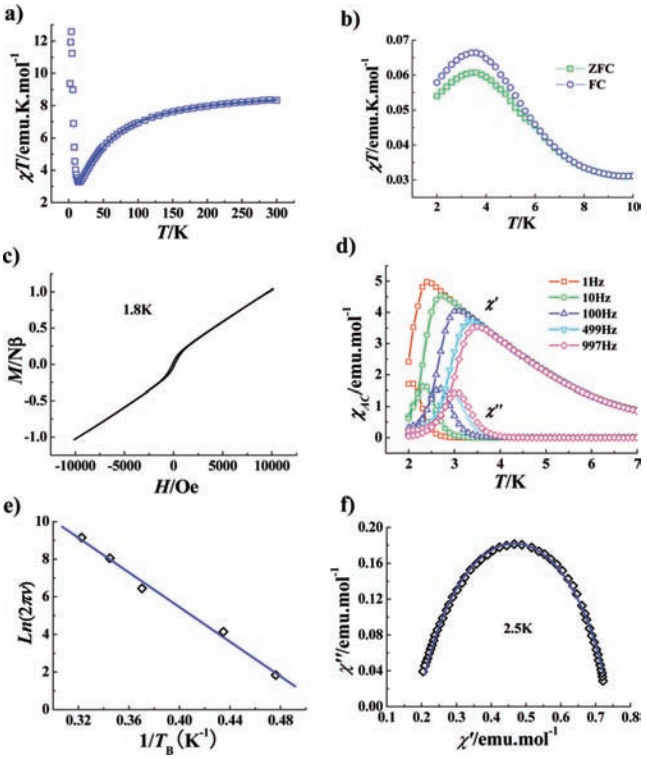

Figure 5. Plot of χT versus T of **2** measured under 1 kOe (a). The solid line represents the best theoretical fitting. Plots of FC and ZFC χT values for **2** (b). Hysteresis loop at 1.8 K for **2** (c). Real χ'' and imaginary χ'' ac magnetic susceptibility as a function of the temperature at different frequencies for **2** (d). The Vogel−Fulcher fit for **2**. The solid line represents the least-squares fit of the experimental data to the Arrhenius law (e). Cole−Cole diagram at 2.5 K for **2**. The solid line represents the least-squares fit obtained with a Debye model (f).

The divergence of the ZFC−FC χT product below 6 K indicates the occurrence of irreversibility of magnetization (Figure 5b). The field-dependent magnetization at 1.8 K displays a small hysteresis with a coercive field of 210 Oe (Figure 5c). The ac susceptibility measurements indicated that both the in-phase susceptibility (χ') and the out-of-phase component (χ'') are strongly frequency-dependent below 4 K (Figure 5d), precluding any three-dimensional ordering. The shift of peak temperature (T_f) of χ'' is measured by a parameter $\Phi = (\Delta T_f/T_f)/\Delta(\log \omega) = 0.17$; this value is 2 orders of magnitude larger than that for a canonical spin glass, but closer to a normal value for a superparamagnet.[8] The ac oscillating frequency corresponding to the observed peaks at different temperatures was fit to the Arrhenius law, $\tau = \tau_0 \exp(\Delta E/k_B)$, giving $\tau_0 = 4.3(1) \times 10^{-11}$ S and $\triangle/k_B = 46(2)$ K (Figure 5e), suggesting a thermally activated mechanism. At 2.5 K, a semicircle Cole−Cole diagram was obtained (χ'' vs χ', Figure 5f), as expected for a Debye model with a single relaxation time (τ).[9,10] The best fitting gives an α parameter of 0.256, indicating a narrow distribution of

(8) Mydosh, J. A. *Spin Glasses, An Experimental Introduction*; Taylor and Francis: London, 1993.

(9) (a) Cole, K. S.; Cole, R. H. *J. Chem. Phys.* **1941**, *9*, 341. (b) Boettcher, C. J. F. *Theory of Electric Polarization*; Elsevier: Amsterdam, **1952**. (c) Aubin, S. M.; Sun, Z.; Pardi, L.; Krzysteck, J.; Folting, K.; Brunel L.-J.; Rheingold, A. L.; Christou, G.; Hendrickson, D. N. *Inorg. Chem.* **1999**, *38*, 5329.

(10) In a Debye model, the ac susceptibility, $\chi_{ac}(\nu) = \chi'(\nu) + i\chi''(\nu)$, is given by the following relation: $\chi_{ac}(\nu) = \chi_{ac}(\nu \rightarrow 0)/\{1 + i[2\pi\nu \cdot \tau(T)]\}$.

relaxation times. The dynamics of the magnetization relaxation of **2** are reminiscent of those of typical single-chain magnets, where the energy barrier originates from the magnetic anisotropy.[3]

The dc susceptibility of **3** shows similar behaviors to that of **2** (Figure 6a). The χT product decreases continuously from the room temperature value of 8.38 emu·K·mol^{-1} and falls rapidly when $T < 100$ K upon cooling, reaching a minimum at 14 K. Below 14 K, χT increases to a maximum at 6 K, with a value of 5.70 emu·K·mol^{-1}, then falls. The susceptibility data above 20 K were well-fitted to the Curie−Weiss law, with $C = 9.48$ cm^3 mol^{-1} K and $\Theta = -37.50$ K.

Analysis of the χT data above 20 K using the same model [an isosceles triangle (J_1, J_2) model] as for **1** and **2** gives $J_1 = -0.72$ cm^{-1}, $J_2 = -3.13$ cm^{-1}, $zJ = -0.18$ cm^{-1}, and $g = 2.02$ with $R = 1.51 \times 10^{-4}$. Irreversibility was observed in the ZFC and FC χT product below 3.0 K (Figure 6b). The field dependence of the magnetization measured at 1.8 K gives a coercive field of 420 Oe (Figure 6c), two times that of **2**. The ac susceptibility data for **3** in the temperature range 2−8 K show a strong frequency dependence in both χ' and χ'' (Figure 6d), precluding any three-dimensional long-range ordering. The Φ value of 0.14 is also a normal value for a superparamagnet.[8] The frequency dependence of the peak temperatures of χ'' can be fitted well to the Arrhenius law, with $\tau_0 = 4.41 \times 10^{-11}$ S and $\triangle/k_B = 57(1)$ K (Figure 6e). A semicircle Cole−Cole diagram was obtained at 3.0 K (Figure 6f), which was fitted by a Debye model[9,10] giving an α parameter of 0.271, comparable with that of **2** ($\alpha = 0.256$). The dynamics of the magnetization relaxation of **3** suggest a classical SCM behavior too.

There are three octahedral configuration Mn^{3+} ions in the [$Mn_3^{III}O$] unit of both **2** and **3**, with their JT elongation axes nearly parallel to each other and to the chain directions; such arrangements can enhance the uniaxial anisotropy of the chains: one essential requirement for a SCM. On the other hand, the absence of the Mn···Br short contact weak interaction that was observed in **1** suggests a weak interchain coupling in **2** and **3**, which can meet with another requirement for an SCM, that is, good isolation of the chains. Therefore, the evident SCM-type behaviors of **2** and **3** are expected. Furthermore, the diversity of SCMs' behaviors can be ascribed roughly to the subtle structural differences between **2** and **3**, such as the slightly shorter Mn···carboxylato···Mn separation and the better isolation of the chains in **3** with respect to **2**.

Conclusions

Three stepwise chain complexes based on the anti−anti carboxylato-bridged [$Mn_3^{III}O(Brppz)_3$] units were structurally and magnetically characterized. The solvents have great influences on not only the stoichiometry of the stepwise chain products but also their magnetic properties. Either a methanol or ethanol molecule can take part in the coordination, situating at the JT elongation axis position of the coordination configurations of the Mn^{3+} ions. There are three methanol molecules on the remaining coordination sites of two octahedral configuration manganese(III) ions in **1** but four ethanol molecules on the JT elongation axis sites of the three octahedral configuration

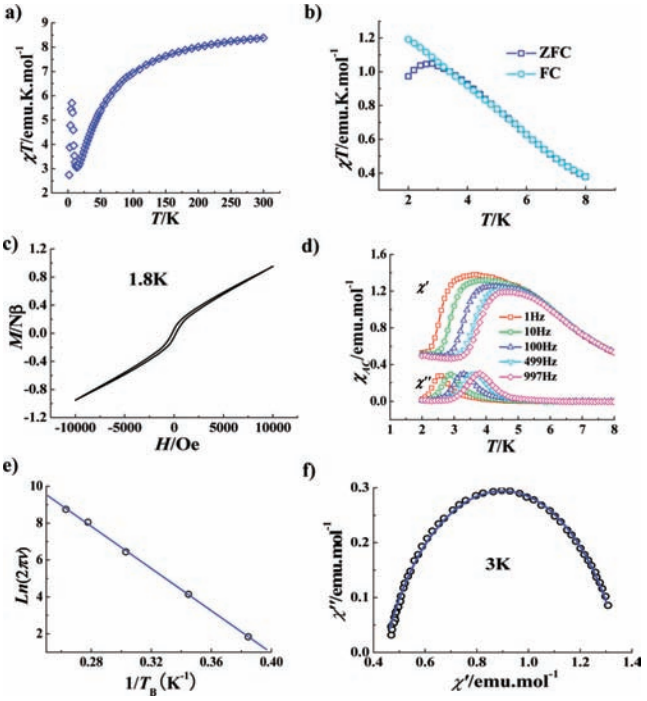

Figure 6. Plot of χT versus T of **3** measured under 1 kOe (a). The solid line represents the best theoretical fitting. Plots of FC and ZFC χT value for **3** (b). Hysteresis loop at 1.8 K for **3** (c). Real χ' and imaginary χ'' ac magnetic susceptibility as a function of temperature at different frequencies for **3** (d). The Vogel−Fulcher fit for **3**. The solid line represents the least-squares fit of the experimental data to the Arrhenius law (e). Cole−Cole diagram at 3 K for **3**. The solid line represents the least-squares fit obtained with a Debye model (f).

manganese(III) ions in **2** and **3**. Consequently, the anisotropy-enhanced [$Mn_3^{III}O$] units owing to three parallel JT elongation axes are formed in **2** and **3** with respect to **1** in which only two manganese(III) ions have octahedral configurations. This can meet with the critical requirement for an SCM, that is, the existence of uniaxial anisotropy in the unit, which is ultimately intended to be an Ising chain. This is one reason why **2** and **3** display SCM behaviors. Furthermore, the presence of the interchain Mn···Br short contact weak interactions in **1** is propitious to show a long-range magnetic ordering. The presence of the interchain short contact weak interactions in **1** but their absence in **2** and **3** is another important reason for **1** and **2** or **3** to show quite different magnetic properties at low temperatures. This work provides a family of 1D chain complexes based on the same unit, the same coligand, and the same bridging ligand for studying the modulation of magnetic properties via solvents' coordination role. Furthermore, the polymorphs as observed for **2** and **3** will enrich the field of SCMs.

Acknowledgment. This work was supported by National Natural Science Foundation of China (20671093 and 20473096), the Major State Basic Research Development Program of P. R. China (2006CB932101), and Chinese Academy of Sciences.

Supporting Information Available: X-ray crystallographic data in CIF format for **1**−**3**, CCDC-6660421 (**1**), CCDC-696163 (**2**), and CCDC-696164 (**3**). This material is available free of charge via the Internet at http://pubs.acs.org.